

## Random-walk simulations of flow in Hele Shaw cells

Shoudan Liang

*Department of Physics and The James Franck Institute, The University of Chicago, 5640 South Ellis Avenue, Chicago, Illinois 60637*

(Received 24 June 1985)

An algorithm related to diffusion-limited aggregation is used to generate patterns of interface motion in the Hele Shaw geometry. With increasing surface tension, the objects generated change from fractal structures to smooth boundary "fingers." The fingers' profiles agree with experiments and numerical solutions. The fingers' width as the function of the surface tension is consistent with the results obtained through other simulational methods. As the surface tension is decreased, apparently unstable patterns of flow develop. For very small values of the surface tension, a kind of dendritic growth is produced.

### I. INTRODUCTION

Interfacial stability and pattern formation are common in many physical problems.<sup>1,2</sup> One of the simplest examples is the Saffman-Taylor problem<sup>3</sup> which involves the displacement of water by air between two pieces of closely spaced rectangular glass sealed at two long edges—a two-dimensional geometry originally considered by Hele Shaw.<sup>4</sup>

As in many other problems, the surface tension tends to stabilize an interface, which is driven under an external force and would otherwise be unstable. As the result of the competition between two forces, static patterns may form. When the driving force increases, the pattern becomes time dependent. Then, under appropriate conditions, an oscillatory and highly branched pattern called a dendrite will form.

Typically, the equations of motion for the interface in these problems are simple. But they are not easy to solve, even numerically. Thus, in a similar but more difficult problem, directional solidification, several serious attempts have been made to simplify the problem to make it numerically tractable.<sup>5,6</sup>

Recently, a random-walk model has been introduced to attack these problems.<sup>7</sup> It is based on a model originally invented by Witten and Sander<sup>8</sup> as a means to generate fractal structures. The model, called diffusion-limited aggregation (DLA), has particles diffuse from far away toward an existing cluster, which then attach to it at the point of first contact. DLA generates a ramified and chaotic structure.

To simulate the hydrodynamic experiments with the random-walk generated structures, we must face two problems: we must reduce the randomness in the random walk simulations because the motion of the interface is deterministic; and we must include surface tension in the simulations. The first problem may be solved by letting random walkers strike many times before a particle is attached to the cluster.<sup>9</sup> For the second problem, two methods can be used. In one method, the probability that a random walker sticks to the cluster depends on the local radius of curvature.<sup>7</sup> In another method, particles are al-

lowed to walk off the cluster with a probability proportional to the local curvature.<sup>10</sup> The second method has a clear mathematical interpretation,<sup>10</sup> and thus is the better means to achieve the effect of the surface tension.

The purposes of this paper are to carry out the ideas put forward in Ref. 10, and to examine the random-walk model by applying it to the Saffman-Taylor problem. An algorithm is constructed that approximates the Saffman-Taylor problem to any degree of accuracy. The control parameter is derived, and its correctness is confirmed by testing it against the known results of linear stability analysis. The quantitative results from the simulations are compared and found to be in agreement with conformal mapping<sup>11</sup> and boundary integral<sup>12</sup> methods, as well as with the experiments. The algorithm also preserves rigorously the incompressibility of the fluids.

Section II is devoted to the physical problem to be simulated. We then specify in Sec. III the details of the random-walk algorithm. Section IV deals with a few tricks used in the simulations. In Sec. V, we report various tests on the algorithm. Finally, Sec. VI summarizes the results of the simulations.

### II. BASIC EQUATIONS

In this section, we state the equations describing the Saffman-Taylor problem. They can all be derived directly from the Navier-Stokes equation.

A Hele Shaw cell is composed of two pieces of closely spaced glass sealed at both edges (Fig. 1). Initially it is filled with water. Air is then pushed in from the "bottom" to displace the water. If the plates are horizontal, gravity is irrelevant. We are interested in the interface between air and water. When the gap between the two pieces of glass  $b$  is small, the velocity of the water  $\mathbf{v}$  is proportional to the pressure gradient<sup>3</sup>

$$\mathbf{v} = -\frac{b^2}{12\mu} \nabla p, \quad (1)$$

where  $\mu$  is the fluid viscosity.

Assuming that the fluids are incompressible,  $\nabla \cdot \mathbf{v} = 0$ , we get, combining with Eq. (1),

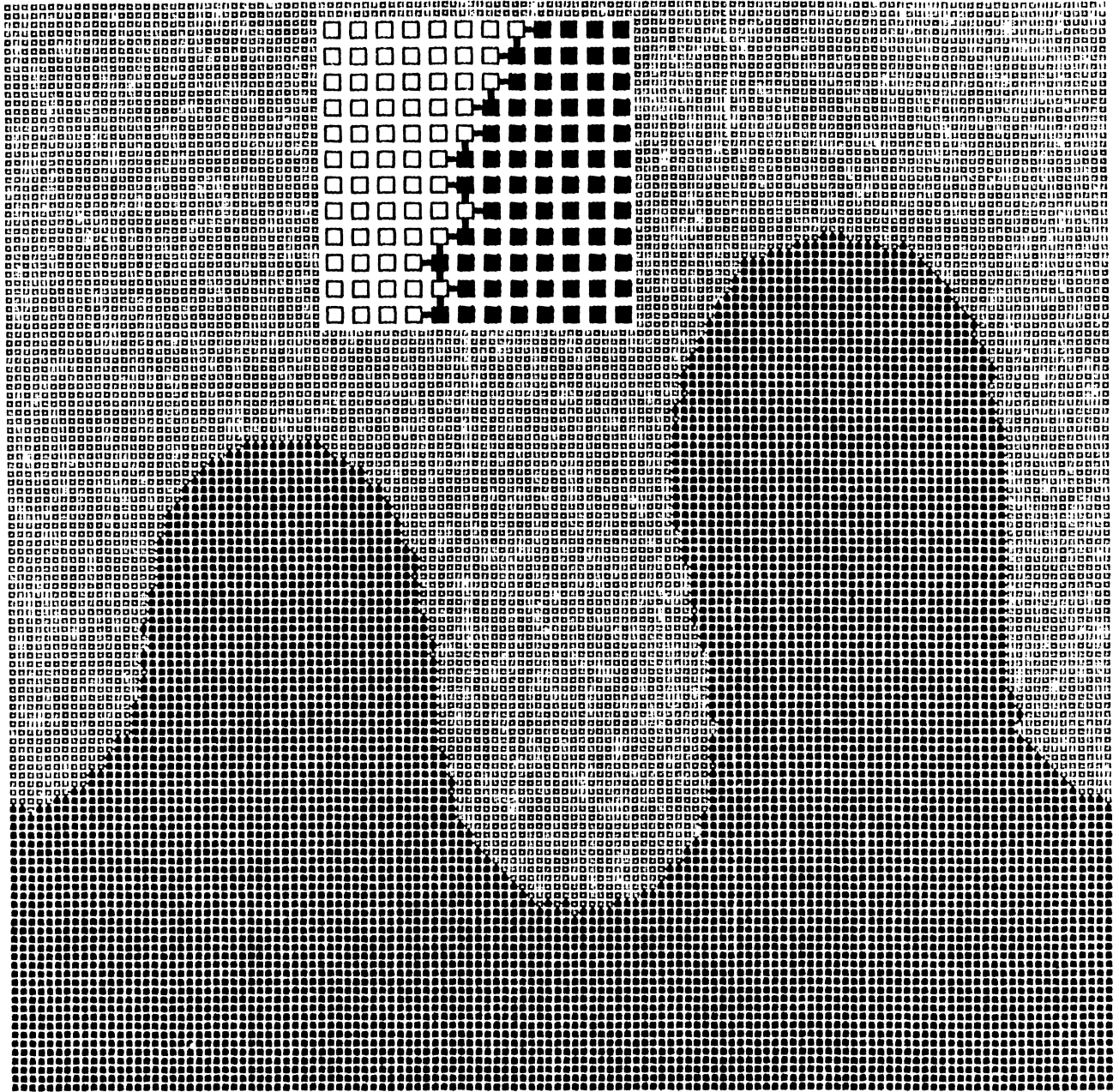


FIG. 1. Darker region represents a thin layer of air in a Hele Shaw cell and the lighter region represents water. Random walks take place in the white region. Bonds are connected between every pairs of adjacent sites on different regions (see the insert), and they contain numbers. The air-water interface moves in accordance with these numbers. While all random walks end at the interface, they may start either from a horizontal line above the interface which provides an upward pressure gradient, or from the interface itself, which rearranges the interface and represents surface tension.

$$\nabla^2 p = 0. \quad (2)$$

A curved interface introduces a pressure difference between air and water

$$\Delta p = \frac{T}{R} + p_0, \quad (3)$$

where  $T$  is the surface tension parameter, and  $R$  is the radius of curvature. Air is much less viscous than water. So the pressure in the air is about constant. The above condition reduces to

$$p_{\text{interface}} = \frac{T}{R} + p_0. \quad (4)$$

To Eqs. (1)–(3) we need to add two boundary conditions. The walls are impenetrable

$$(\nabla p)_n |_{\text{walls}} = 0 \quad (5a)$$

and the water flows at a constant rate far away from the interface

$$\mathbf{v}|_{y \rightarrow \infty} = V_0 \hat{\mathbf{y}}, \quad (5b)$$

where  $\hat{\mathbf{y}}$  is the unit vector in the  $y$  direction.

Experimentally, when the air is pushed, a flat air-water interface first ripples. Then the instability grows. Small fluctuations develop into a random structure of many small fingers (Fig. 2). Because on the one hand the pressure in the water is constant, and at the same time the equal pressure line in the water far away from the interface is flat, the finger penetrating into the water most will feel the greatest pressure gradient and will thus be most

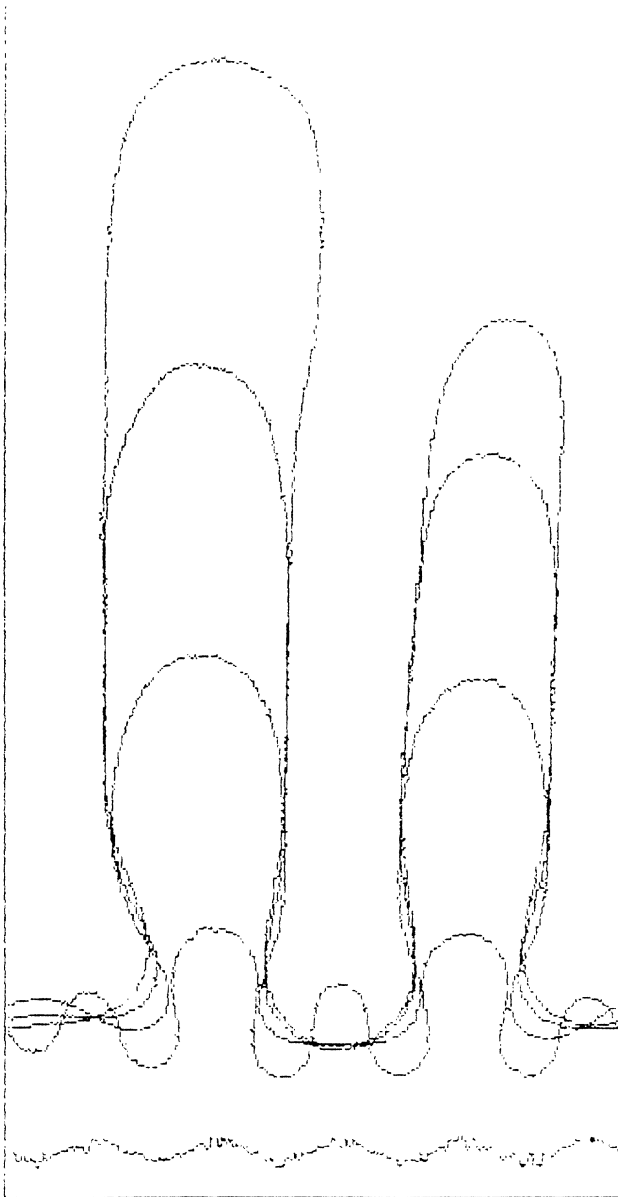


FIG. 2. Perturbations first grow to small fingers, then the biggest finger takes over while the smaller ones shrink. The channel's width is 254 lattice units, and  $B=0.001$ , at which the unstable wavelength is about one-fifth of the channel's width.

likely to grow. Then, this finger emerging out of the chaotic pattern then becomes stable again. It eventually goes to the center of the channel and advances at a constant velocity without changing its symmetric profile.

$\lambda$ , the ratio of the finger's width to the width of the channel, is determined by a dimensionless parameter  $B$ , defined by Tryggvason and Aref as<sup>13</sup>

$$B = \frac{1}{W^2} \frac{T}{\frac{12\mu}{b^2 V_0}}, \quad (6)$$

where  $W$  is the width of the channel.

Later, we will derive the corresponding  $B$  for the random-walk algorithm.

### III. ALGORITHM

It is well known that the probability distribution of a random walker satisfies the Laplace equation. Since the pressure in a Hele Shaw cell satisfies the same equation, it is possible to draw an analogy between the probability distribution of a random walker and the pressure field in the Hele Shaw cell.<sup>8-10,14-16</sup> When the appropriate conditions are satisfied at the boundary, i.e., the random walkers are released with certain probabilities from the boundary, the pressure in the Hele Shaw cell is just the number of times random walkers visit various sites.

Just as in the diffusion-limited aggregation simulation, our algorithm has occupied and unoccupied sites, representing air and water. Random walks take place in the unoccupied region and are confined to a rectangular box. The most interesting region is, of course, the interface separating the air and the water.

To solve the Laplace equation for the field  $p$  in a region, it is enough to specify the value of the field at the boundary. In particular, the solution may be expressed as a sum over a geometry-dependent Green's function  $g(r,s)$  weighted by the boundary value  $\Psi(s)$

$$p(r) = \sum_s g(r,s) \Psi(s),$$

where the sum runs over all points on the boundary.  $g(r,s)$  is the electric field generated by a point source located at  $s$  on a grounded conductor.

It is shown in Ref. 10 that the Green's function  $g(r,s)$  is proportional to the number of times the point  $r$  in the unoccupied region is visited by the random walkers which are released from the point  $s$  on the interface and end whenever they hit any occupied site again. In this problem, the boundary is naturally divided into two regions. At the interface, the boundary value is given by Eq. (4); far away from the interface, the gradient of the field is specified in Eqs. (5b) and (1). Corresponding to the two kinds of boundaries, there are two types of "walks." In the first type of walk, particles come from "infinity" and terminate at a point on the interface where the cluster

grows. As will be shown later, this type of walk represents the constant pressure gradient far away from the interface. It carries flux from the outside. The second type of walk leaves a point  $s$  on the interface with probability  $\Psi(s)$  and ends at possibly another point on the interface.  $\Psi(s)$  is given by

$$\Psi(s) = \frac{T}{R_s} + p_0, \quad (7)$$

where  $R_s$  is the radius of curvature, and  $T$  determines the surface tension.  $p_0$  is irrelevant and can have any value. This type of walks transfers flux from one part of the interface to another, thus it changes the shape of the interface.

As we have seen, the interface may move both forward and backward. To achieve this effect in the simulation, it is convenient to connect bonds between every occupied and unoccupied site at the interface, as shown in Fig. 1. The total number of net crossings of random walkers through each bond is recorded as numbers. These numbers determine the motion of the interface. Roughly speaking, one waits until the absolute value of the number for a bond reaches a previously assigned value  $M$ , then the interface moves forward or backward according to the sign of the number.

This rule can be understood in a simple way. Let  $N_s$  be the number of times random walkers have visited the site  $s$ . Since the probability a random walker goes to any one of its four neighbors  $r$  is  $1/4$ , the number of net crossings of random walkers through the bond between  $s$  and  $r$  is  $(N_s - N_r)/4$ . However, the gradient of the pressure is proportional to the local velocity of the interface. The accumulated flux is equivalent to the integration of the velocity over time, which is the area the interface sweeps out per unit length. Thus a certain amount of flux is equivalent to the motion of the interface by one lattice site. This rule is enforced in the actual simulations. For an unoccupied site on the interface, the positive flux of all bonds connecting with it is added. When the sum is larger than  $M$ , the site is occupied. On the other hand, for the occupied site on the interface, all negative flux is added. When the sum is smaller than  $-M$ , the site is emptied. In both cases, the interface moves. The purpose of introducing  $M$  is to average over many walkers in order to reduce the randomness.

Notice that random walks from the interface to itself always conserve flux. This implies, through the rules of the interface motion, that area occupied by a fluid is conserved, or the fluid is incompressible. The surface tension can only change the shape of the interface but not the area included by it.

There is one difficulty in interpreting Eq. (7). The radius of curvature  $R_s$  can be positive or negative but the probability  $\Psi(s)$  should always be positive. This difficulty is solved by letting each walker carry a "flux"  $f$  and set, instead of Eq. (7),

$$f\Psi(s) = \frac{T}{R_s} + p_0 \quad (8)$$

and let  $R_s$  and  $f$  have the same sign. Thus, the probabilities of releasing walkers  $\Psi(s)$  are always positive. When a random walker carrying a flux  $f$  passes through a bond,  $f$  is added to the bond if the walker goes from air to water, and subtracted from the bond if it goes in the other direction.

The dimensionless parameter  $B$  characterizes the competition of the surface tension with the external force. It must be a function of the probability ratio of the two types of walks introduced earlier. In fact, we will show that

$$B = \frac{1}{W^2} \frac{T}{4P_t}, \quad (9)$$

where the probability of the random walkers arriving from the infinity is  $WP_t$ , and the probabilities of the random walkers being released from the sites at the interface are given by Eq. (7).

To prove (8), we recognize that the combination  $12\mu/b^2V_0$  in the denominator of Eq. (6) is the pressure gradient far away from the interface  $\nabla P_{y \rightarrow \infty}$ . Thus

$$B = \frac{1}{W^2} \frac{T}{\nabla P_{y \rightarrow \infty}}.$$

Because of the analogy between the probability distribution of random walkers and the pressure in the Hele Shaw cell, Eqs. (1)–(5) are solved when the boundary value Eq. (7) is used. So one only need show that far away from the interface the pressure gradient is constant, and  $\nabla P_{y \rightarrow \infty} = 4P_t$ . Now, since all the random walks stop at the interface, the ones starting from it do not contribute to the gradient of the field far away. All the contributions come from the random walks starting from infinity. When one such walker is released, there will be, on average, a probability  $1/W$  that it passes any vertical bond in the  $y$  direction. However, the number of net crossings of

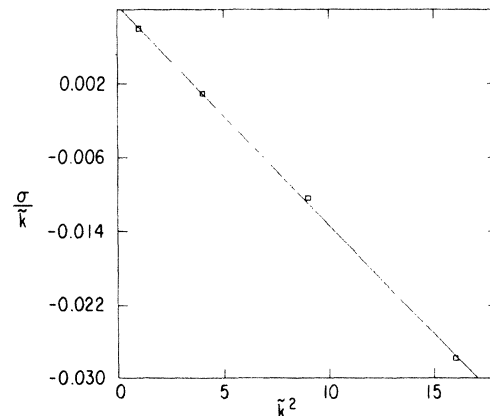


FIG. 3. A plot of  $\sigma/\bar{k}$  vs  $\bar{k}^2$  [Eq. (10)]. The growth rate  $\sigma$  is on an arbitrary scale.  $B$  is determined by the wave number at which the  $\sigma$  vanishes. This gives  $B = 0.0057$ , while the value of  $B$  calculated by Eq. (9) is 0.006.

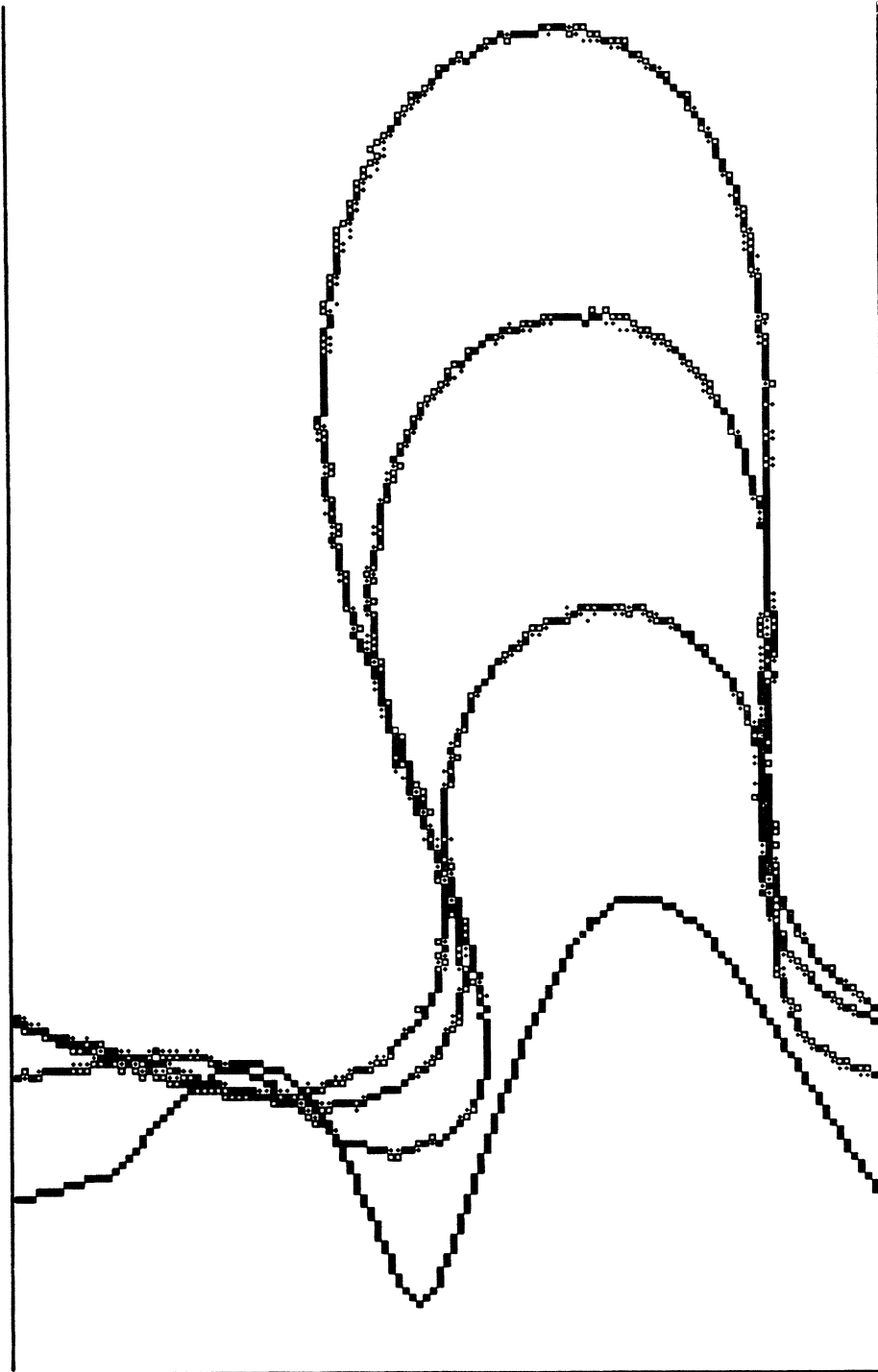


FIG. 4. Comparison of two runs of different random sequences (shown by empty boxes and points) from the same initial condition. The parameters used here are  $B = 0.008$ ,  $M = 15$ ,  $W = 126$ .

random walkers through a bond is one-quarter the difference of the total number of times they visit two sites which connect with the bond. Thus, the gradient of the probability field  $\nabla P_{y \rightarrow \infty}$  is  $4(WP_t)/W$ , which completes the proof.

When  $B$  is large, there are many surface rearrangements, and the interface tends to be flat. When  $B$  is small, we have only walkers added from the outside. The interface will then be unstable, and we will have the fractal structure of DLA.

## IV. SIMULATIONS

A large percentage of the random walks are of the second type, which transfer flux between the sites on the interface. For typical values of  $B$  (about  $10^{-2}$ ) and the channel's width  $W$  (128 lattice units), the probability ratio of the two types of random walks is quite large [ $T/(W/2)/P_t \sim 8BW \sim 10$ ]. It is therefore necessary to have an efficient algorithm to start random walks from the interface. To improve the efficiency, the positions for the occupied sites on the interface are stored in a one-dimensional array. Thus, all the sites on the interface can be assessed easily [the random walkers start from the sites in this array with the probabilities determined by Eq. (7). If they walk to an occupied site, they stop]. The indices to this array also serve as the indices to the array that records flux in bonds. To provide a cross reference, the indices are stored in the array which identifies the occupied and unoccupied sites at the locations of the interface. When the interface moves, these arrays are changed accordingly.

For a smooth finger, the curvature has a maximum  $R_t^{-1}$  at the tip. The probability  $\Psi(s)$  of Eq. (8) is normalized to one at the tip; although fluctuations may generate

some curvature larger than  $R_t^{-1}$ , in which case the magnitude of the flux carried by the random walkers will be increased from the average value  $\bar{f}$ . For small curvature ( $R^{-1} < R_t^{-1}$ ), the absolute value of flux is set to  $\bar{f}$ .

Since not all random walkers carry the same flux, it may happen that accumulated flux stored in bonds is not exactly  $M\bar{f}$ . In our simulation, the "extra" flux is transferred to nearby sites after moving the interface.

There is an arbitrary constant  $p_0$  in Eq. (7). When it is set to zero, the body of the finger, where the interface is relatively flat, has only a few random walkers coming in and out; most random walks take place near the finger's tip where the shape of the interface is constantly changing.

There are several ways to estimate the radius of curvature  $R_s$  for a surface site  $s$ . The simplest one<sup>8</sup> is to count  $N_s$ , the number of sites occupied by air, within a distance  $L$  from  $s$ . Obviously  $N_s$  is related to  $R_s$ . To find out this relation, the sites inside the circle of radius  $R > L$  are occupied. Counting with a computer,  $N_s$  is obtained for each site on the circle, and they are then summed over *bonds* to get the average  $N(R)$ . The air may occupy the sites outside the circle to obtain  $N(R)$  for negative  $R_s$ .

We found that for both positive and negative radius of

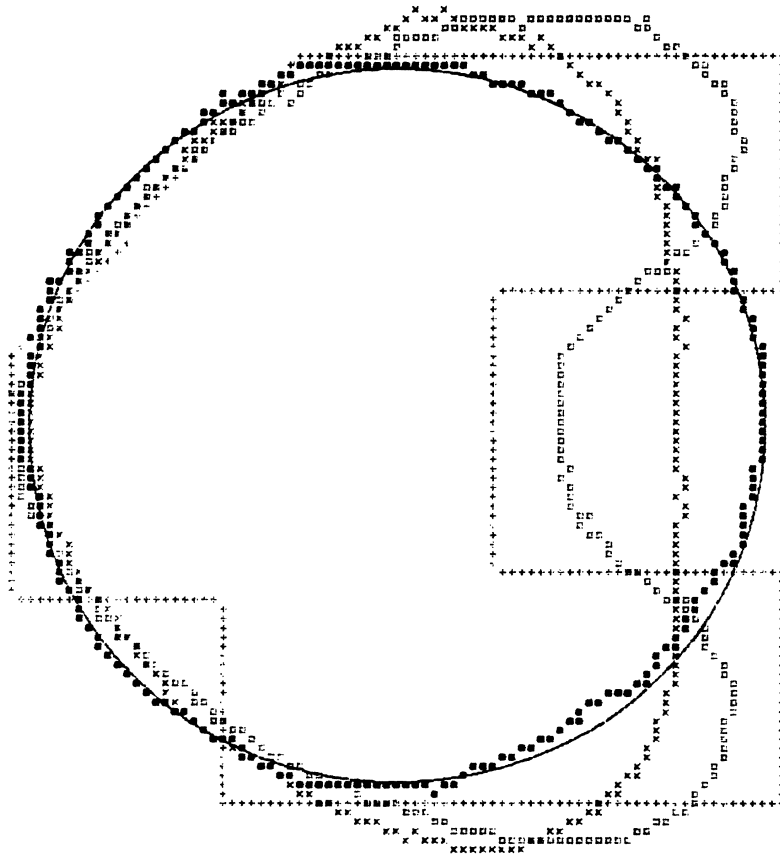


FIG. 5. To prove the surface tension effect, an oddly shaped "air bubble" (shown by crosses) is placed in the water (random walks take place outside the bubble). Empty boxes,  $\times$ 's, and solid boxes represent the shape of the bubble at 0.1, 0.3, and 2.5 million releases of random walkers from the surface of the bubble. A circle (the solid line) is added for comparison. Note that the area of the bubble is conserved.

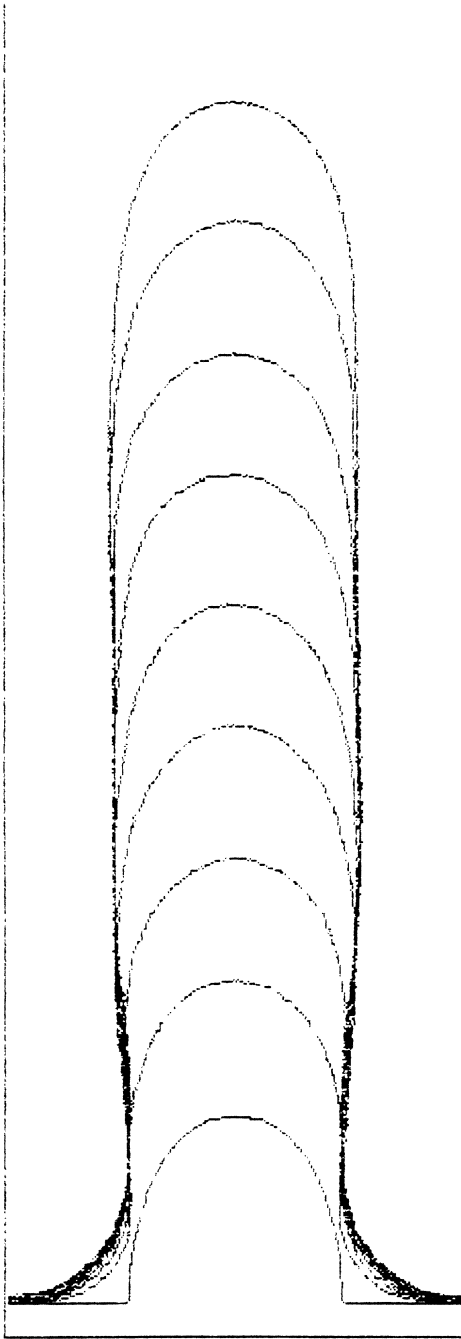


FIG. 6. Time evolution of a finger in the Hele Shaw cell. The channel's width is 254 lattice units  $B=0.005$ ,  $M=10$ , and  $L=10$ ; periodic boundary conditions are used on the side walls. This took 60 CPU hours on a Sun Workstation.

curvature,  $R$  and  $N(R)$  are simply related

$$\frac{1}{R} = \frac{1}{R_L} [N(R) - N_L],$$

where  $R_L$  and  $N_L$  are two constants depending on  $L$ . For  $L$  and  $R$  going to infinity,  $R_L = L^3/3$  and  $N_L = \pi L^2/2$ . For smaller values of  $L$ , we measure them as functions of

surface curvature and average the results.

Two kinds of boundary conditions are employed on the side walls, reflecting and periodic. Both of them are used in our simulations. No difference between them has been detected.

The first type of the random walks need not necessarily come from infinity. Since the random walkers coming from infinity have the same chance to hit any sites on a horizontal line (line with constant  $y$ ) for the first time, they may be released uniformly from any horizontal line above the cluster.

Random walkers that go far away from the interface can be eliminated by returning them back to the relevant region using known probabilities calculated beforehand (see Ref. 10), as we have done in this simulation.

## V. TESTS

Our model can be checked against the linear instability analysis of Saffman and Taylor<sup>3</sup> who predict a growth rate  $\sigma$  for a disturbance of wavelength  $W/\tilde{k}$  on a flat interface<sup>13</sup>

$$\sigma = 2\pi\tilde{k}[1 - B(2\pi\tilde{k})^2], \quad (10)$$

where  $\tilde{k}$  is the reduced wave vector, an integer in the present case.

If the sine waves with the integer wave vector  $\tilde{k}$  are superimposed on the flat interface at the initial time, the position of the interface at a later time should be

$$y = V_0 t + A_0 e^{\sigma t} \sin[2\pi\tilde{k}(x/W)].$$

The first term, the mean position, sets the time in an arbitrary unit. Our simulations do show that the amplitude of the sine wave grows exponentially when  $A_0$  is not too large, and  $\sigma/\tilde{k}$  is proportional to  $\tilde{k}^2$  (Fig. 3). The wave number  $\tilde{k}^*$  at which the growth rate vanishes determines the control parameter

$$B = \frac{1}{(2\pi\tilde{k}^*)^2}.$$

$B$  measured in this way agrees with calculations of Eq. (9).

In a Monte Carlo simulation, the result may become unreliable because of the random noise. In this simulation, noise can be reduced by increasing the average number  $M$ , or  $W$ , the number of lattice sites across the channel.

At reasonably large  $M$  and large  $B$ , we get reproducible results. For example, when  $M=15$ ,  $W=126$ ,  $B=0.008$  and the initial condition is a nonsymmetric double bump, the agreement between two runs of entirely different random sequences is satisfactory (Fig. 4) after the interface advances a distance  $W$ . Two runs of  $M=10$  and  $M=15$  agree well when other conditions are fixed.

A square lattice introduces some anisotropy. To see how big it is we can put a "air bubble" in the water. If we do not add random walkers from the outside and only allow the interface-to-interface walks, the air bubble will adjust itself and eventually takes its equilibrium shape—a

circle. Figure 5 shows an oddly shaped air bubble developing into a circle.

### VI. RESULTS

Figure 6 shows a typical finger at large surface tension. It is stable and symmetric. Unlike the case in Fig. 2,

where the initial state is a chaotic pattern, the finger in Fig. 6 starts from a symmetric curve. But, as both the experiments and the simulations have shown, the differences in the initial conditions do not change the finger's shape at the late stage of its development. The unique shape depends only on the control parameter  $B$ .

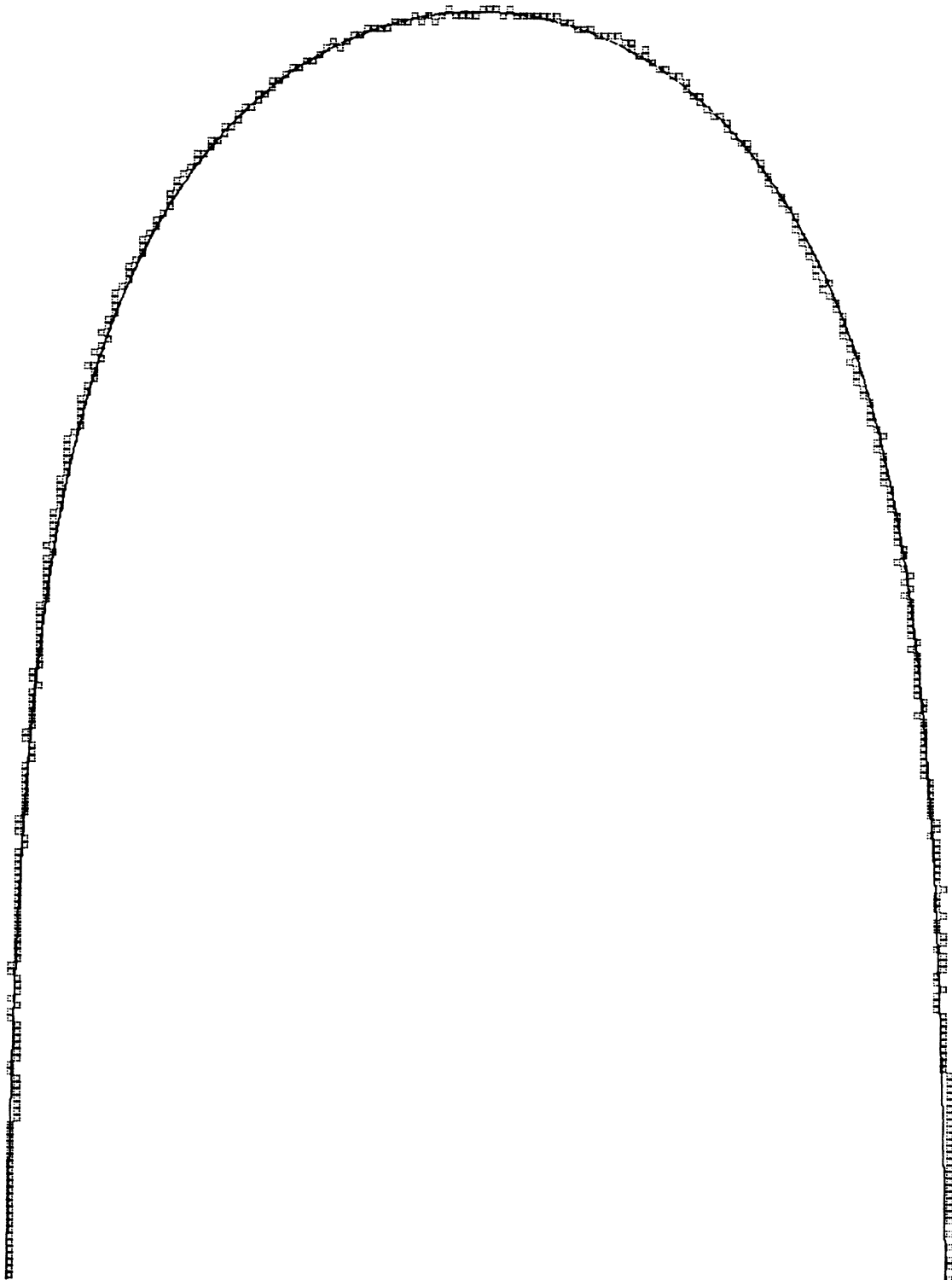


FIG. 7. Profile (shown as boxes) of the last finger in the time series depicted in Fig. 6 is compared with a curve calculated from Pitts' phenomenological scaling hypothesis (solid line) which is placed at the center of the channel. The size of the boxes is the resolution of the underlying lattice. ( $B = 0.005$ ,  $\lambda = 0.55$ ,  $M = 10$ .)

As the finger moves faster, its width becomes narrower. It has been shown in the experiments that at large velocity, or small value of  $B$ , the width ratio of the finger to the channel  $\lambda$  approaches one-half. Over a large range of velocities, the fingers' width  $\lambda$  is about one-half and the fingers take almost the same shape. Saffman and Taylor<sup>3</sup> have found a family of solutions to Eqs. (1)–(5) at zero surface tension. The profile of one half-width finger observed in their experiments agrees well with their solution at  $\lambda = \frac{1}{2}$ . Moreover, as Pitts<sup>17</sup> has pointed out, fingers of all widths are simply related. Take the profile of the one-half finger, scale it in both  $x$  and  $y$  directions by  $2\lambda$ ; the resulting curve is indistinguishable from the experimental finger of width  $\lambda$  if  $\lambda$  is not too close to one. Figure 7 compares our simulation with Pitts' scaling hypothesis and shows a good agreement between the two.

When the finger is stable, the  $\lambda$  is uniquely determined by the control parameter  $B$ . McLean and Saffman<sup>18</sup> have solved numerically for the static profile of the interface. They found that the  $\lambda$  depends only on  $B$ . Conformal mapping<sup>11</sup> and boundary integral<sup>12</sup> methods have also been used to attack this problem. The time evolution of a finger can be followed, and the stable fingers have been found. Unlike the zero surface tension case, the width of stable fingers is not arbitrary and depends only on  $B$ . The functional form agrees with McLean-Saffman simulations.

Despite the presence of white noise, our simulations give rise to stable fingers. To measure the width of the fingers, one can, of course, read the width directly from the finger. A more sophisticated method is to record the number of occupied sites along with the height of the finger's tip. They are linearly related. The slope determines the finger's width ratio  $\lambda$ . The results of this measurement at several values of  $B$  are shown in Fig. 8. The bigger circle used in curvature measuring seems to give a better result because the small circle is not sensitive to small curvatures.

If the interface is to be stable, the noise must be kept within certain limits. The amount of noise is controlled by the  $M$  defined previously. In our simulation, the averaging number  $M$  changes from around 10 for  $B > 0.02$  to about 50 for  $B$  close to 0.001. Although the small  $M$  tends to widen the finger, simulations show  $\lambda$  does not change when  $M$  is large enough. A typical error in  $\lambda$  is about three percent for different runs. Because the number of lattice points across the channel is finite, large  $M$  may introduce another kind of error. When a particle sticks to the tip of the finger, the tip grows a finite amount. This in turn "shields" the pressure field and makes it harder for the body of the finger to grow. This effect is large at the small channel's width and large  $M$ , because the large fluctuations at small  $M$  depress this effect. The fact that small  $M$  in our simulations tends to give  $\lambda$  more in agreement with other simulations may be due to this effect. But, as we shall see later, larger  $\lambda$  could also mean that the unstable regime is reached. Each point in Fig. 8 is obtained from a stable finger grown to a length of four times the channel's width.

Both reflecting and periodic boundary conditions are used on the side walls. No difference has been observed

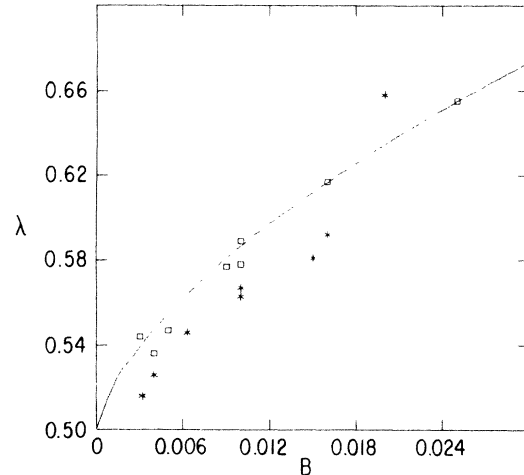


FIG. 8. Finger's width  $\lambda$  as a function of the control parameter  $B$ . The solid line is McLean and Saffman's numerical result. Boxes represent the fingers' width when  $L$  is 10, and stars when  $L$  is 3.2.  $M$  used ranges from 10 to 15 for boxes and 15 to 25 for stars except for two stars close to the solid line, for which  $M = 7$ .

for  $\lambda < 0.7$ .

When properly used, the initial conditions can help to reduce the computational time. One could start from a flat interface, but it is not a good choice, because the interface has to waste time in becoming unstable and then stable again. Also, when  $B < 0.0253$  (where the critical unstable wavelength is equal to the channel's width), no disturbance can grow. So we used initial conditions that are already roughly in a finger's shape, or at least not flat.

Because of the Monte Carlo characteristic of the algorithm, noise effects are inevitable in our simulation. As we have mentioned before, at large values of  $B$ , the small amount of noise built into our calculation does not change the final shape of the profile. This suggests that the stable finger has a certain domain of attraction in the solution space. Within this domain small disturbances die out. Only when the amplitude of noisy perturbations exceeds a threshold value, does it have a chance to grow. Bensimon<sup>11</sup> has argued that this noise threshold  $v_c$  is extremely sensitive to the control parameter  $B$ ; he shows that  $v_c = \exp(-\gamma B^{-\beta})$  where  $\beta = 0.61$ , and  $\gamma = 0.076$ . Because of the finite resolution of the lattice, the minimum noise we have here is  $1/W$  which means for any reasonable lattice width used in the simulation ( $10^2$  to  $10^3$ ) [The computation time grows roughly as  $W^2(1+BW)$  with the channel's width  $W$  in lattice units.] The finger is always unstable when  $B$  is below 0.001. Bensimon also finds the three most unstable modes. Two of them are asymmetric and oscillatory. The other one is a symmetric steady mode corresponding to a wider or narrower finger. At large  $B$ , we have observed the wider finger at small averaging number  $M$ .

At small  $B$ , where the noise threshold is small, the finger is unstable in two senses. One possibility is that the process is not reproducible. The profile at the time  $t$  depends crucially on the initial conditions, the particular

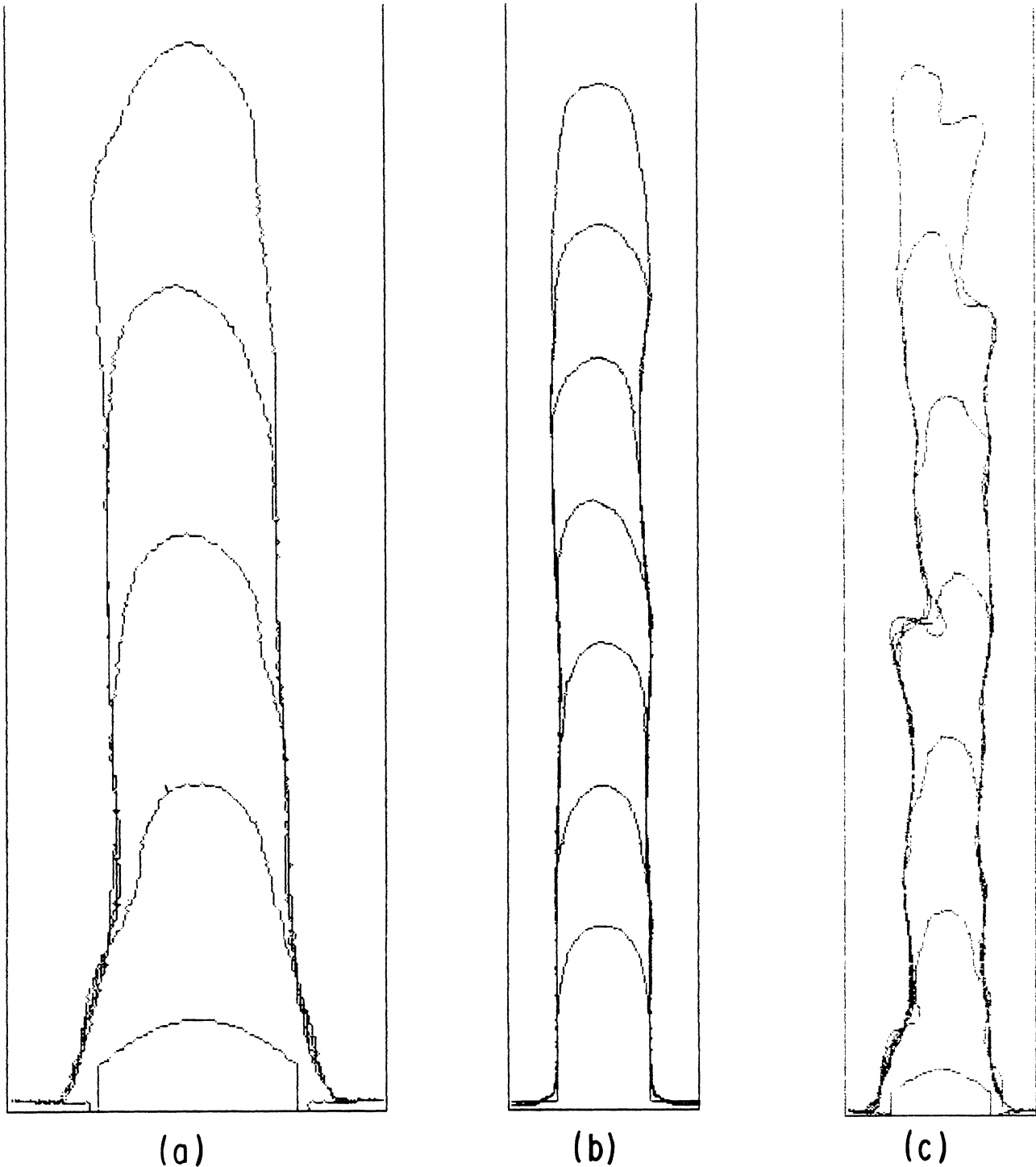


FIG. 9. Some unstable modes are shown here. The reflecting boundary condition was used in all cases. (a) At the onset of instability, the finger becomes symmetric. ( $B = 1.8 \times 10^{-3}$ ,  $M = 20$ .) (b) A finger with an oscillatory trace as a result of the finger's switching from the one side of the center to the other. ( $B = 2.4 \times 10^{-3}$ ,  $M = 25$ .) (c) Plateaus trigger the tip splitting. ( $B = 8 \times 10^{-4}$ ,  $M = 10$ .) (d) The finger's tip splits. ( $B = 4 \times 10^{-4}$ ,  $M = 15$ .) (e) A finger with side branches. ( $B = 4 \times 10^{-5}$ ,  $M = 50$ .) (f) A DLA-like structure. ( $B = 5 \times 10^{-6}$ ,  $M = 3$ .)

random sequence used, and the value of  $M$ . Another possibility is that the unstable finger has a time-dependent shape. Our simulation seems to suggest that the unstable modes depend on the ratio of the noise amplitude to the noise threshold. As this ratio becomes larger, the finger

first becomes slightly asymmetric, then the finger's tip splits. After that, one observes an oscillatory mode, and finally many side branching and a DLA-like structure.

Figure 9 shows some of the unstable modes. At the onset of the instability, the finger's tip goes off the center of

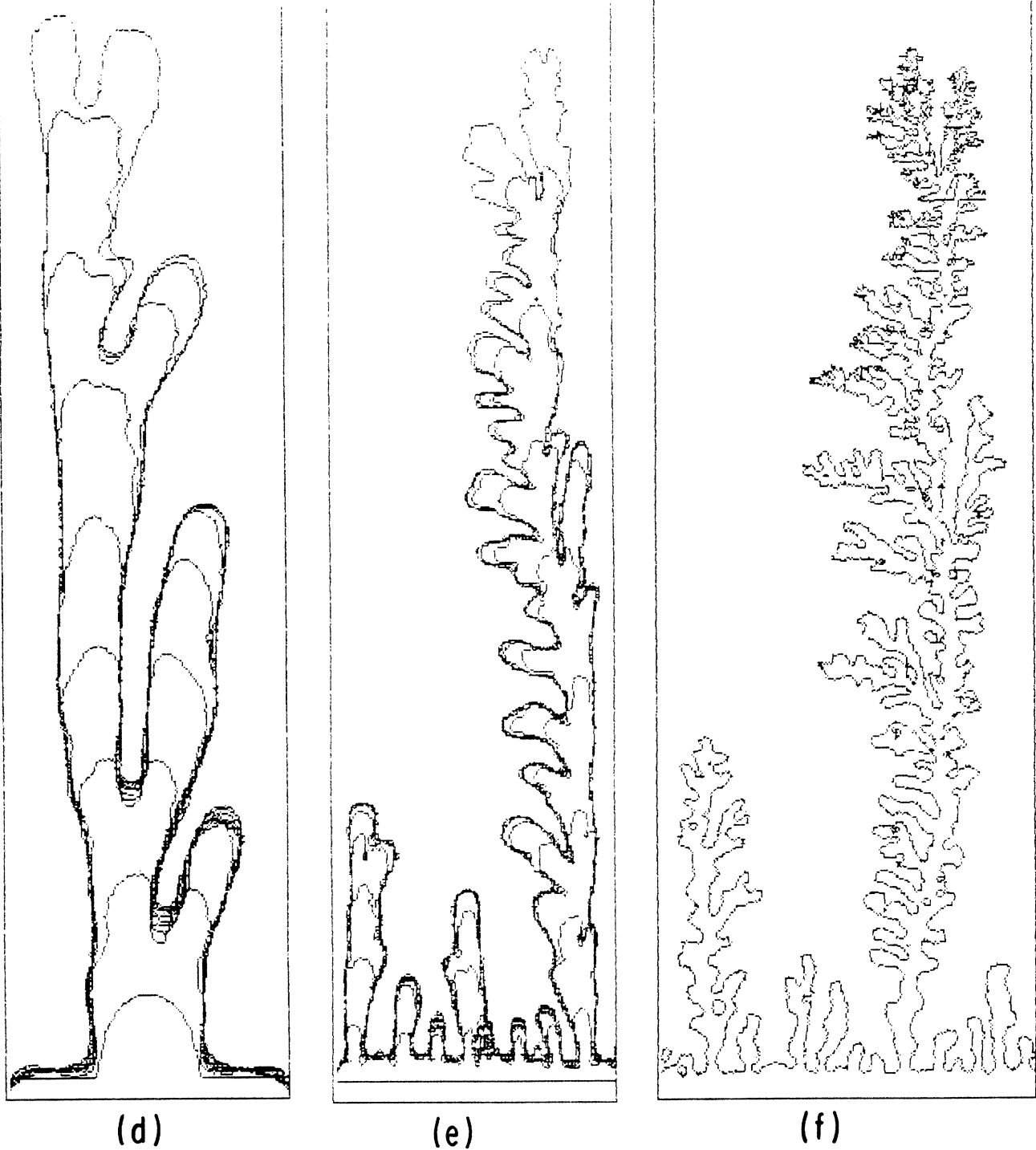


FIG. 9. (Continued).

the channel. As the noise increases, the tip can switch from one side of the center to the other leaving a swinging trace behind. If the noise is increased further, the finger's top develops to a tip and a plateau which is likely to trigger a finger splitting. At very small  $B$ , when the noise's ratio to the noise threshold  $\nu_c$  is large, the sides of the finger cease to be stable. Side branches grow out.

Some of those unstable patterns are similar to experimental observations.<sup>19</sup>

The wavelength of the side branches in our simulations is proportional to  $\sqrt{B}$ . This is similar to the prediction of linear instability analysis for the unstable mode growing from an initially flat interface. The simulations also show that the wavelength of the side branches is three to four

times  $\lambda_c$ , the wavelength below which no disturbances on a flat interface can grow.

At small  $B$ , the interface is unstable because of noise. Experimentally, Maher measured the length of the mixing zone<sup>13,20</sup>  $\theta$  defined as the distance along the direction of flow between the tips of the longest fingers in each direction. He found that, for  $B$  ranging from  $10^{-3}$  to  $10^{-5}$ ,  $\theta$  has a power-law dependence on time  $t$ ,  $\theta \sim t^{1.6}$ . The exponent 1.6 is an averaged value of exponents measured at different  $B$ .

We have tried to fit our simulated  $\theta$  to the power law. With  $W=254$  lattice units,  $B=10^{-4}$ , and  $M$  around 10, the fitting is rather poor, and  $\theta \sim t^{1.6}$ , for  $\theta$  between  $0.2W$  and  $2W$ . The data for  $M=50$  at the same  $B$  gave a worse fit to the power-law form, especially at early time. At  $B=10^{-5}$  and  $M=10$ , the fitting becomes better, and the exponent is 1.3. When  $\theta$  is much larger than  $W$ , it grows linearly with time.

We also measured  $h$ , the distance from the tip of the longest finger to the initial interface. When  $h$  is neither too large nor too small, we found  $h \sim t^{1.35}$ . Notice that at  $B=0$  and  $M=1$ , our model is identical to DLA. For a DLA cluster, this index would be  $1/(D-1)=1.4$  (where  $D$  is the fractal dimension for a DLA cluster in two dimensions),<sup>21</sup> since time is proportional to the number of occupied sites. This suggests that at small  $B$ , the flow pattern is like DLA. If the flow pattern depends only on  $B$ , then one should observe a DLA-like structure in very large cells.

## VII. CONCLUSIONS

We have applied the random-walk model to the Saffman-Taylor problem. An explicit algorithm is given which combines the right form of surface tension and a way of averaging out noise. Simulations are performed. The resulting finger profiles agree with experiments and with other types of simulations. The dependence of the finger's width on the surface tension also agrees with the stationary calculation of McLean and Saffman as well as with the conformal mapping and the boundary integral methods.

## ACKNOWLEDGMENTS

I am grateful to my thesis advisor L. P. Kadanoff for his advice and insights; to C. Tang for introducing me to the problem and for giving me much help; and to P. Tabeling for showing me the experimental data prior to publication and for many useful conversations. I would also like to thank D. Bensimon, M. Jensen, A. Libchaber, Z. Qiu, S. Sarkar, and B. Shraiman for many stimulating discussions. T. C. Halsey and T. Rosenbaum helped me improve the manuscript. This work was supported by U.S. Department of Energy and the National Science Foundation and made use of the Sun Workstations of the Materials Research Laboratory and the Department of Astrophysics at The University of Chicago. It is in partial fulfillment for the Ph.D. requirement at The University of Chicago.

<sup>1</sup>J. S. Langer, *Rev. Mod. Phys.* **52**, 1 (1980).

<sup>2</sup>T. K. Perkins, O. C. Johnston, and R. N. Hoffman, *Soc. Pet. Eng. J.* **5**, 301 (1965).

<sup>3</sup>P. G. Saffman and G. I. Taylor, *Proc. R. Soc. London, Ser. A* **245**, 312 (1958).

<sup>4</sup>J. H. S. Hele Shaw, *Nature* **58**, 34 (1898).

<sup>5</sup>E. Ben-Jacob, Nigel Goldenfeld, J. S. Langer, and Gerd Schon, *Phys. Rev. A* **29**, 330 (1984).

<sup>6</sup>R. Brower, D. Kessler, J. Koplik, and H. Levine, *Phys. Rev. Lett.* **51**, 1111 (1983).

<sup>7</sup>T. Vicsek, *Phys. Rev. Lett.* **53**, 2281 (1984).

<sup>8</sup>T. A. Witten and L. M. Sander, *Phys. Rev. Lett.* **47**, 1400 (1981); *Phys. Rev. B* **27**, 5686 (1983).

<sup>9</sup>C. Tang, *Phys. Rev. A* **31**, 1977 (1985).

<sup>10</sup>L. P. Kadanoff, *J. Stat. Phys.* **39**, 267 (1985).

<sup>11</sup>D. Bensimon, *Phys. Rev. A* **33**, 1302 (1986).

<sup>12</sup>A. J. DeGregoria and L. W. Schwartz, *J. Fluid Mech.* (to be published).

<sup>13</sup>G. Tryggvason and H. Aref, *J. Fluid Mech.* **136**, 1 (1983); and (unpublished).

<sup>14</sup>L. Paterson, *Phys. Rev. Lett.* **52**, 1621 (1984).

<sup>15</sup>J. Nittman, G. Daccord, and H. E. Stanley, *Nature* **314**, 141 (1985).

<sup>16</sup>J. Szep, J. Cserti, and J. Kertesz (unpublished).

<sup>17</sup>E. Pitts, *J. Fluid Mech.* **97**, 53 (1980).

<sup>18</sup>J. W. McLean and P. G. Saffman, *J. Fluid Mech.* **102**, 455 (1981).

<sup>19</sup>P. Tabeling and A. Libchaber, *Phys. Rev. A* **33**, 794 (1986).

<sup>20</sup>J. V. Maher, *Phys. Rev. Lett.* **54**, 1498 (1985).

<sup>21</sup>Leo P. Kadanoff, private communication.